ChemComm

COMMUNICATION

View Article Online
View Journal | View Issue

Cite this: *Chem. Commun.*, 2015, **51**, 5610

Received 16th December 2014, Accepted 8th January 2015

DOI: 10.1039/c4cc09999k

www.rsc.org/chemcomm

A microporous metal–organic framework with rare lvt topology for highly selective C_2H_2/C_2H_4 separation at room temperature†

Hui-Min Wen,[a] Bin Li,*[a] Hailong Wang,[a] Chuande Wu,[b] Khalid Alfooty,[c] Rajamani Krishna[d] and Banglin Chen*[ac]

A new lvt-type metal–organic framework UTSA-60a with suitable pore channels and open metal sites has been developed for highly selective separation of C_2H_2/C_2H_4 at room temperature.

In steam cracking of ethane to produce ethene, ethyne is one of the small amounts of by-products, which has a deleterious effect on end-products of ethene such as polyethene; therefore, it is imperative to remove ethyne from ethene. Typically, the impurity level of 40 ppm C_2H_2 needs to be met for ethene feed for the polymerization reactor. The main commercial methods to eliminate ethyne from crude ethene include partial hydrogenation and solvent extraction which are costly and energy-intensive.[1] One of the alternative and energy-efficient strategies for this separation is adsorptive separation technology using porous materials. Although traditional porous zeolites and activated carbons have been extensively examined for this very important separation, no porous materials have been realized to significantly differentiate these two gas molecules.[2]

Porous metal–organic frameworks (MOFs), which can be readily self-assembled from metal ions/clusters with organic linkers,[3] have been rapidly emerging as a new class of porous materials for gas storage and separation applications.[4,5] Judicious selection of molecular building blocks can tune their structures, pore/window sizes, and functionalization at the molecular level to optimize and thus fulfill their specific separation of small molecules.[6] Recently, the potential utility of porous MOFs for separation of hydrocarbon mixtures has been explored by a number of independent groups.[7,8] Among the diverse gas separations, separation of C_2H_2/C_2H_4 is one of the most challenging and difficult ones because of their similar sizes, volatilities, and electronic structures.[9] To the best of our knowledge, only a few microporous MOFs have been realized for this separation so far.[10–13] For example, our group realized a series of microporous mixed MOFs (MMOFs) for highly selective separation of C_2H_2/C_2H_4 by fine tuning of pore sizes.[10] Long and Chen's groups independently reported that a series of MMOF-74 (M = Mg, Fe, and Co) with high density of open metal sites can separate C_2H_2 from the mixture well.[11,12] However, the MMOFs suffer from the low C_2H_2 uptake capacities due to the narrow pore windows, while the MMOF-74 materials need significantly high regeneration energy costs to overcome the strong binding energy between open metal sites and gas molecules. Apparently, there is an increasing demand to develop better adsorbents with both high selectivity and C_2H_2 uptake but low regeneration cost to fulfill this challenging separation. With this in mind, we developed a novel tetracarboxylic acid ligand (H_4BTAA, Scheme 1), and reported herein the synthesis of its first porous MOF (termed as UTSA-60) with suitable window sizes and open Cu^{2+} sites for such a purpose.‡ This material exhibits not only higher C_2H_2/C_2H_4 selectivity and C_2H_4 productivity, but also lower regeneration energy costs compared to MMOF-74 (M = Mg, Fe, and Co), featuring it as one of the best adsorbents for selective separation of C_2H_2/C_2H_4 at room temperature.

The organic linker H_4BTAA, benzene-1,2,4,5-tetraacrytic acid, was simply synthesized by Heck cross-coupling reactions

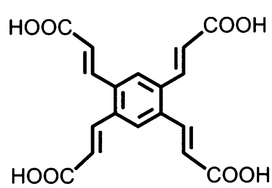

Scheme 1 The organic ligand H_4BTAA for the construction of UTSA-60.

[a] Department of Chemistry, University of Texas at San Antonio, One UTSA Circle, San Antonio, Texas 78249-0698, USA. E-mail: banglin.chen@utsa.edu, bin.li@utsa.edu; Fax: +1-210-458-7428
[b] Department of Chemistry, Zhejiang University, Hangzhou 310027, China
[c] Department of Chemistry, Faculty of Science, King Abdulaziz University, Jeddah, Saudi Arabia
[d] Van't Hoff Institute for Molecular Sciences, University of Amsterdam, Science Park 904, 1098 XH Amsterdam, The Netherlands

† Electronic supplementary information (ESI) available: Synthesis and characterization of UTSA-60, PXRD, TGA, sorption isotherms, and breakthrough simulations. CCDC 1038935. For ESI and crystallographic data in CIF or other electronic format see DOI: 10.1039/c4cc09999k

of 1,2,4,5-tetraiodobenzene and methyl acrylate, followed by hydrolysis and acidification. Reactions of the organic linker with $Cu(NO_3)_2 \cdot 2.5H_2O$ in acidified DMF–H_2O at 60 °C for 24 h afforded green block crystals of UTSA-60. The as-synthesized UTSA-60 can be formulated as $[Cu_2BTAA(H_2O)_2] \cdot 2DMF \cdot 2H_2O$, as determined by single-crystal XRD analysis, TGA and elemental analysis. The phase purity of the bulk material was also confirmed by powder X-ray diffraction (Fig. S3, ESI†).

Single-crystal X-ray diffraction analysis revealed that UTSA-60 crystallizes in the orthorhombic space group *Imma*. As frequently observed in MOFs, the framework nodes in UTSA-60 consist of paddle-wheel dinuclear $Cu_2(COO)_4$ secondary building units (SBUs) with the organic linkers to form a three-dimensional (3D) framework (Fig. 1a). UTSA-60 shows a rarely observed lvt-type network of $4^2 \cdot 8^4$ topology which is different from the well-known nbo MOFs (Fig. 1b).[14] There exist three types of open channels of about 4.8 × 4.0 Å^2 along the *b* axis, 3.6 × 2.8 Å^2 along the *c* axis, and 3.7 × 10.5 Å^2 along the *a* axis, respectively.

Of most interest are the small channels along the *b* axis, which present a large number of unsaturated Cu^{2+} centers for the recognition of gas molecules (Fig. 1d). As a result, the combined feature of small pore channels and open metal sites within UTSA-60a highlights its potential for highly selective adsorptive separation of C_2H_2–C_2H_4 mixtures.

Prior to gas adsorption measurements, the as-synthesized UTSA-60 was solvent-exchanged with dry acetone, and then evacuated at 273 K for two days and at room temperature for 2 h under high vacuum to yield the activated UTSA-60a. The PXRD analysis indicates that the activated UTSA-60a retains its crystalline feature (Fig. S3, ESI†), although the peaks of UTSA-60a are slightly different from those of the as-synthesized UTSA-60 due to the flexible nature of double-bond spacers in the organic linker.[15] The permanent porosity was established by nitrogen sorption at 77 K. The N_2 sorption isotherm at 77 K exhibits a typical Type-I sorption behaviour, characteristic of a microporous material (Fig. S6, ESI†). The Brunauer–Emmett–Teller (BET) and Langmuir surface areas were estimated to be 484 and 500 m^2 g^{-1}, respectively.

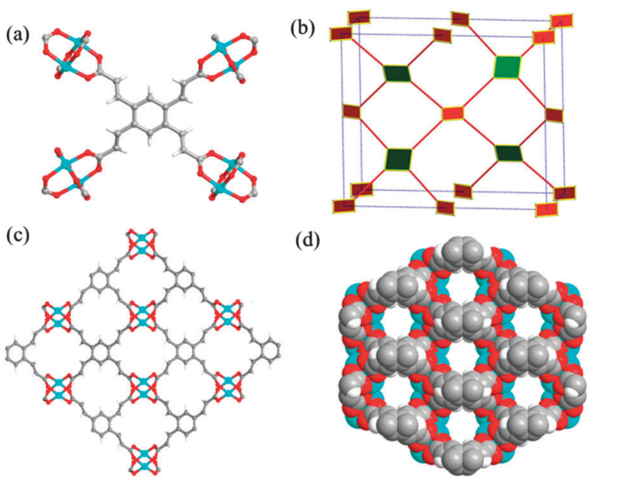

Fig. 1 X-ray single crystal structure of UTSA-60, indicating that (a) each tetracarboxylate ligand connects with four paddle-wheel $Cu_2(COO)_4$ clusters; (b) the framework topology of the lvt net; (c) the structure viewed along the *c* axis, indicating the pore channels of about 3.6 × 2.8 Å^2; and (d) the pore channels viewed along the *b* axis indicating the pore channels of about 4.8 × 4.0 Å^2 in diameter (C, gray; H, white; Cu, blue).

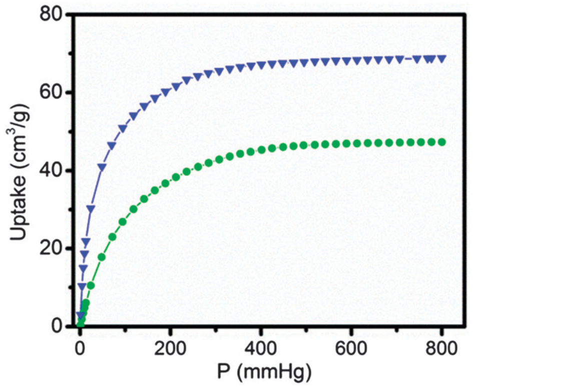

Fig. 2 Single-component adsorption isotherms for C_2H_2 (blue) and C_2H_4 (green) of UTSA-60a at 296 K.

The establishment of permanent microporosity in UTSA-60a prompted us to examine its potential as an adsorbent for the industrially important C_2H_2/C_2H_4 separation. Single-component adsorption isotherms for acetylene and ethylene were measured up to 1 atm at 273 and 296 K, respectively. As shown in Fig. 2, UTSA-60a shows remarkably different adsorption behaviours with respect to C_2H_2 and C_2H_4 at 296 K. The adsorption isotherms of C_2H_2 in UTSA-60a display a rapid increase at low pressure and then saturation at around 30 kPa; however, the uptake of C_2H_4 increases slowly following this pressure. More importantly, UTSA-60a can take up a moderate amount of C_2H_2 (70 cm^3 g^{-1}) at 1 atm and 296 K, which is much higher than the amount of C_2H_4 (46 cm^3 g^{-1}) under the same conditions. These observed discrepancies between C_2H_2 and C_2H_4 absorption properties suggest that UTSA-60a might be a promising candidate for C_2H_2/C_2H_4 separation, which encouraged us to examine its feasibility to selectively separate C_2H_2 from binary C_2H_2–C_2H_4 mixtures in more detail.

Ideal Adsorbed Solution Theory (IAST) was utilized to calculate the adsorption selectivity of UTSA-60a for the binary C_2H_2–C_2H_4 mixtures containing 1% C_2H_2. Fig. 3a presents the IAST calculations of C_2H_2/C_2H_4 adsorption selectivities for UTSA-60a and three other representative MOFs (MMOF-74, M = Mg, Fe, and Co) at 296 K. The adsorption selectivity of UTSA-60a lies in the range of 5.5 to 16 at room temperature, which is significantly higher than those obtained in the range of 1.6 to 2.2 for FeMOF-74, CoMOF-74, and MgMOF-74 with high density of open metal sites. This is really remarkable, featuring UTSA-60a as the unique MOF having the highest adsorption selectivity for C_2H_2/C_2H_4 separation except MMOF-3a.[9,11] Besides adsorption selectivity, uptake capacity of C_2H_2 is also important in determining the performance of any given adsorbent in industrial fixed bed adsorbers. Fig. S8 (ESI†) compares the gravimetric uptake capacity of C_2H_2 for adsorption from mixtures containing 1% C_2H_2. At a total gas phase pressure of 100 kPa, the hierarchy of uptake capacities

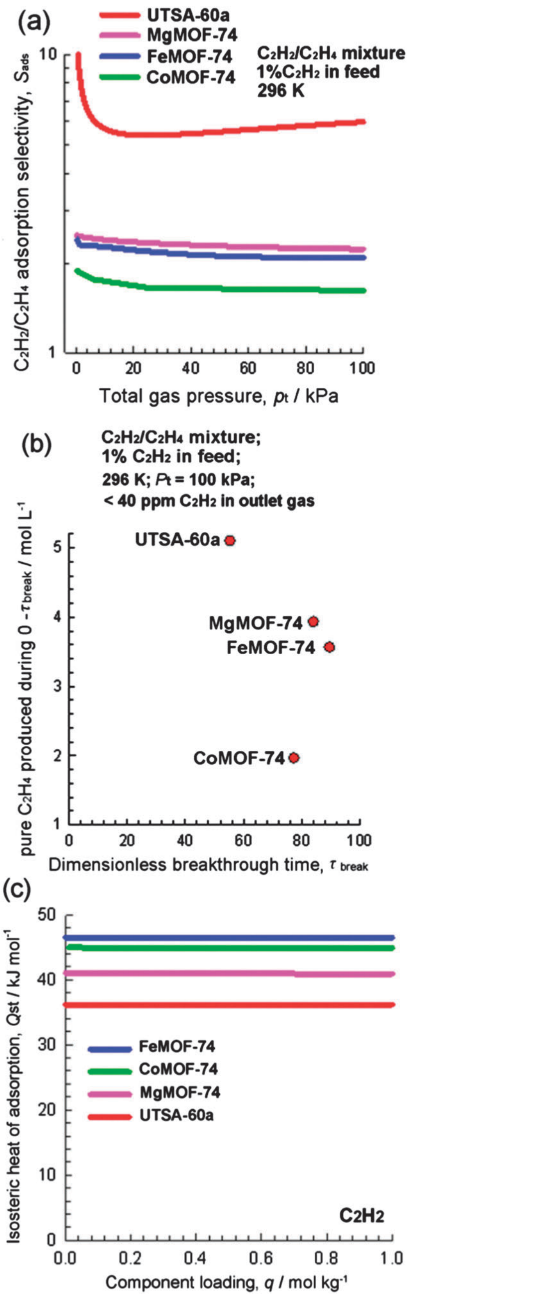

Fig. 3 (a) IAST calculations of C_2H_2/C_2H_4 adsorption selectivities for UTSA-60a, MgMOF-74, FeMOF-74, and CoMOF-74 at 296 K; (b) the plot of pure C_2H_4 produced per L of adsorbent, during the time interval $0 - \tau_{break}$, plotted as a function of the time interval τ_{break}. The temperature is 296 K for all MOFs except FeMOF-74 for which the chosen temperature is 318 K; (c) comparison of isosteric heats of C_2H_2 adsorption, Q_{st}, in UTSA-60a, FeMOF-74, CoMOF-74 and MgMOF-74. The calculations of Q_{st} are based on the use of the Clausius–Clapeyron equation.

for C_2H_2 is MgMOF-74 > FeMOF-74 ≈ UTSA-60a > CoMOF-74. Although the C_2H_2 uptake capacity of UTSA-60a is slightly lower than that of MgMOF-74, the much higher selectivity of UTSA-60a can outweigh its uptake capacity disadvantages. Taken together, UTSA-60a is superior to MMOF-74 in terms of C_2H_2/C_2H_4 separation.

To further validate the feasibility of using UTSA-60a for this separation, transient breakthrough simulations were carried out using the methodology developed and described in the literature (see the ESI† for details).[16] The simulated breakthrough curve of UTSA-60a for the C_2H_2/C_2H_4 separation at 296 K is shown in Fig. S9 (ESI†). It is very clear that UTSA-60a can efficiently separate C_2H_2 from the C_2H_2/C_2H_4 (1/99) mixture at room temperature, in which ethylene breaks through first because of the lower adsorptivity relative to acetylene. The breakthrough time, τ_{break} of UTSA-60a, which satisfies the required purity level of 40 ppm, can be determined in Fig. S10 (ESI†). We note that pure C_2H_4 can be collected during the time interval, which can satisfy the feedstock requirements of the polymerization reactor in the polymer industry. From a material balance on the adsorber, the amount of C_2H_4 (of the required purity <40 ppm C_2H_2) produced during the time interval $0 - \tau_{break}$ can be determined. A plot of the amount of C_2H_4 produced as a function of the time interval τ_{break} is presented in Fig. 3b. Importantly, the hierarchy of the productivity of pure C_2H_4 is UTSA-60a > MgMOF-74 > FeMOF-74 > CoMOF-74, further highlighting that UTSA-60a shows better separation performance than MMOF-74. The superior performance of UTSA-60a is mainly attributable to the significantly higher C_2H_2/C_2H_4 adsorption selectivity as witnessed in Fig. 3a.

On the basis of the data presented in Fig. S10 (ESI†), the impurity level will meet the desired purity level of 40 ppm (indicated by the dashed line) after a certain time, τ_{break}. The adsorption cycle needs to be terminated at that time τ_{break} and the regeneration process needs to be initiated. In this context, the regeneration energy cost of the bed is another very important consideration. Fig. 3c presents a comparison of the heats of adsorption (Q_{st}) of C_2H_2 in UTSA-60a with three other selected MOFs. It is worthy of note that the value of Q_{st} in UTSA-60a is much lower than that of MgMOF-74, FeMOF-74 and CoMOF-74; this implies that the regeneration energy requirement of UTSA-60a will be less than those of MMOF-74, thus leading to significant energy saving. Such lower Q_{st} of C_2H_2 for UTSA-60a is probably attributed to its significantly lower concentration of open metal sites (3.18 mmol cm^{-3}) relative to MgMOF-74 (7.15 mmol cm^{-3}), FeMOF-74 (7.28 mmol cm^{-3}), and CoMOF-74 (7.25 mmol cm^{-3}).

In conclusion, we have developed and characterized a new porous MOF UTSA-60a with lvt topology for highly selective separation of C_2H_2–C_2H_4 mixtures at room temperature. The foregoing results demonstrated that UTSA-60a shows not only much higher selectivity and C_2H_4 productivity, but also lower regeneration costs than those of MMOF-74 (M = Mg, Fe, and Co), highlighting its superior performance for this industrially important separation. Such high separation capacity of UTSA-60a is mainly attributed to the suitable pore windows and open metal sites around channel surfaces of the framework to differentiate both gas molecules. The breakthrough simulations further indicated that this material is able to separate C_2H_2 from the C_2H_2/C_2H_4 (1/99) mixture at room temperature, in which the purity requirement of 40 ppm in the outlet gas can be readily achieved using the fixed bed UTSA-60a adsorber.

This work was supported by the Welch Foundation (AX-1730).

Notes and references

‡ Crystal data for UTSA-60: $C_{18}H_{14}Cu_2O_{10}$, M = 517.37, orthorhombic, space group *Imma*, a = 18.8261(10) Å, b = 22.1934(9) Å, c = 10.0062(8) Å, V = 4180.7(4) Å^3, Z = 4, D_c = 0.822 g cm^{-3}, F(000) = 1040.0, final R_1 = 0.0639 for $I > 2\sigma(I)$, wR_2 = 0.1700 for all data, GOF = 0.948, CCDC 1038935.

1 (*a*) N. A. Khan, S. Shaikhutdinov and H.-J. Freund, *Catal. Lett.*, 2006, **108**, 159; (*b*) K. Weissermel and H.-J. Arpe, *Industrial Organic Chemistry*, Wiley-VCH, Weinheim, 4th edn, 2003, p. 91.
2 (*a*) A. J. Kodde, J. Padin, P. J. van der Meer, M. C. Mittelmeijer-Hazeleger, A. Bliek and R. T. Yang, *Ind. Eng. Chem. Res.*, 2000, **39**, 3108; (*b*) W. K. Lewis, E. R. Gilliland, B. Chertow and W. Milliken, *J. Am. Chem. Soc.*, 1950, **72**, 1157.
3 (*a*) O. M. Yaghi, M. O'Keeffe, N. W. Ockwig, H. K. Chae, M. Eddaoudi and J. Kim, *Nature*, 2003, **423**, 705; (*b*) S. Kitagawa, R. Kitaura and S.-i. Noro, *Angew. Chem., Int. Ed.*, 2004, **43**, 2334; (*c*) J.-P. Zhang, Y.-B. Zhang, J.-B. Lin and X.-M. Chen, *Chem. Rev.*, 2012, **112**, 1001; (*d*) H. Furukawa, K. E. Cordova, M. O'Keeffe and O. M. Yaghi, *Science*, 2013, **341**, 6149; (*e*) Y. He, B. Li, M. O'Keeffe and B. Chen, *Chem. Soc. Rev.*, 2014, **43**, 5618.
4 (*a*) K. Sumida, D. L. Rogow, J. A. Mason, T. M. McDonald, E. D. Bloch, Z. R. Herm, T.-H. Bae and J. R. Long, *Chem. Rev.*, 2012, **112**, 724; (*b*) R. B. Getman, Y.-S. Bae, C. E. Wilmer and R. Q. Snurr, *Chem. Rev.*, 2012, **112**, 703; (*c*) M. P. Suh, H. J. Park, T. K. Prasad and D.-W. Lim, *Chem. Rev.*, 2012, **112**, 782; (*d*) Y. He, W. Zhou, G. Qian and B. Chen, *Chem. Soc. Rev.*, 2014, **43**, 5657; (*e*) B. Li, H.-M. Wen, H. Wang, H. Wu, M. Tyagi, T. Yildirim, W. Zhou and B. Chen, *J. Am. Chem. Soc.*, 2014, **136**, 6207; (*f*) C. E. Wilmer, O. K. Farha, T. Yildirim, I. Eryazici, V. Krungleviciute, A. A. Sarjeant, R. Q. Snurr and J. T. Hupp, *Energy Environ. Sci.*, 2013, **6**, 1158; (*g*) Y. Peng, V. Krungleviciute, I. Eryazici, J. T. Hupp, O. K. Farha and T. Yildirim, *J. Am. Chem. Soc.*, 2013, **135**, 11887.
5 (*a*) J.-R. Li, J. Sculley and H.-C. Zhou, *Chem. Rev.*, 2012, **112**, 869; (*b*) B. Li, H.-M. Wen, W. Zhou and B. Chen, *J. Phys. Chem. Lett.*, 2014, **5**, 3468; (*c*) P. Nugent, Y. Belmabkhout, S. D. Burd, A. J. Cairns, R. Luebke, K. Forrest, T. Pham, S. Ma, B. Space, L. Wojtas, M. Eddaoudi and M. J. Zaworotko, *Nature*, 2013, **495**, 80; (*d*) O. Shekhah, Y. Belmabkhout, Z. Chen, V. Guillerm, A. Cairns, K. Adil and M. Eddaoudi, *Nat. Commun.*, 2014, **5**, 4228; (*e*) S. Xiang, Y. He, Z. Zhang, H. Wu, W. Zhou, R. Krishna and B. Chen, *Nat. Commun.*, 2012, **3**, 954; (*f*) Z. Zhang, Z. Yao, S. Xiang and B. Chen, *Energy Environ. Sci.*, 2014, **7**, 2868; (*g*) N. T. T. Nguyen, H. Furukawa, F. Gándara, H. T. Nguyen, K. E. Cordova and O. M. Yaghi, *Angew. Chem., Int. Ed.*, 2014, **53**, 10645; (*h*) A. Torres-Knoop, R. Krishna and D. Dubbeldam, *Angew. Chem., Int. Ed.*, 2014, **53**, 7774.
6 (*a*) B. Chen, S. Xiang and G. Qian, *Acc. Chem. Res.*, 2010, **43**, 1115; (*b*) C. Wang, D. Liu and W. Lin, *J. Am. Chem. Soc.*, 2013, **135**, 13222; (*c*) S.-T. Zheng, T. Wu, C. Chou, A. Fuhr, P. Feng and X. Bu, *J. Am. Chem. Soc.*, 2012, **134**, 4517; (*d*) T. Li, J. E. Sullivan and N. L. Rosi, *J. Am. Chem. Soc.*, 2013, **135**, 9984; (*e*) G.-Q. Kong, S. Ou, C. Zou and C.-D. Wu, *J. Am. Chem. Soc.*, 2012, **134**, 19851; (*f*) H.-L. Jiang and Q. Xu, *Chem. Commun.*, 2011, **47**, 3351.
7 (*a*) S. J. Geier, J. A. Mason, E. D. Bloch, W. L. Queen, M. R. Hudson, C. M. Browncd and J. R. Long, *Chem. Sci.*, 2013, **4**, 2054; (*b*) P.-Q. Liao, D.-D. Zhou, A.-X. Zhu, L. Jiang, R.-B. Lin, J.-P. Zhang and X.-M. Chen, *J. Am. Chem. Soc.*, 2012, **134**, 17380; (*c*) Y. He, W. Zhou, R. Krishnad and B. Chen, *Chem. Commun.*, 2012, **48**, 11813; (*d*) K. Li, D. H. Olson, J. Seidel, T. J. Emge, H. Gong, H. Zeng and J. Li, *J. Am. Chem. Soc.*, 2009, **131**, 10368; (*e*) C. Y. Lee, Y.-S. Bae, N. C. Jeong, O. K. Farha, A. A. Sarjeant, C. L. Stern, P. Nickias, R. Q. Snurr, J. T. Hupp and S. T. Nguyen, *J. Am. Chem. Soc.*, 2011, **133**, 5228; (*f*) Z. R. Herm, B. M. Wiers, J. A. Mason, J. M. V. Baten, M. R. Hudson, P. Zajdel, C. M. Brown, N. Masciocchi, R. Krishna and J. R. Long, *Science*, 2013, **340**, 960; (*g*) B. Li, Y. Zhang, R. Krishna, K. Yao, Y. Han, Z. Wu, D. Ma, Z. Shi, T. Pham, B. Space, J. Liu, P. K. Thallapally, J. Liu, M. Chrzanowski and S. Ma, *J. Am. Chem. Soc.*, 2014, **136**, 8654.
8 (*a*) H. Wu, Q. Gong, D. H. Olson and J. Li, *Chem. Rev.*, 2012, **112**, 836; (*b*) T. K. Trung, P. Trens, N. Tanchoux, S. Bourrelly, P. L. Llewellyn, S. Loera-Serna, C. Serre, T. Loiseau, F. Fajula and G. Férey, *J. Am. Chem. Soc.*, 2008, **130**, 16926; (*c*) N. Nijem, H. Wu, P. Canepa, A. Marti, J. K. J. Balkus, T. Thonhauser, J. Li and Y. J. Chabal, *J. Am. Chem. Soc.*, 2012, **134**, 15201; (*d*) S. Ma, D. Sun, X.-S. Wang and H.-C. Zhou, *Angew. Chem., Int. Ed.*, 2007, **46**, 2458; (*e*) Y.-S. Bae, C. Y. Lee, K. C. Kim, O. K. Farha, P. Nickias, J. T. Hupp, S. T. Nguyen and R. Q. Snurr, *Angew. Chem., Int. Ed.*, 2012, **51**, 1857; (*f*) K. Liu, D. Ma, B. Li, Y. Li, K. Yao, Z. Zhang, Y. Han and Z. Shi, *J. Mater. Chem. A*, 2014, **2**, 15823; (*g*) Y. Huang, Z. Lin, H. Fu, F. Wang, M. Shen, X. Wang and R. Cao, *ChemSusChem*, 2014, **7**, 2647; (*h*) J. Jia, L. Wang, F. Sun, X. Jing, Z. Bian, L. Gao, R. Krishna and G. Zhu, *Chem. – Eur. J.*, 2014, **20**, 9073; (*i*) Y.-P. He, Y.-X. Tan and J. Zhang, *Chem. Commun.*, 2013, **49**, 11323.
9 (*a*) Z. R. Herm, E. D. Bloch and J. R. Long, *Chem. Mater.*, 2014, **26**, 323; (*b*) B. Li, H. Wang and B. Chen, *Chem. – Asian J.*, 2014, **9**, 1474; (*c*) Y. He, S. Xiang and B. Chen, *J. Am. Chem. Soc.*, 2011, **133**, 14570.
10 (*a*) S. Xiang, Z. Zhang, C.-G. Zhao, K. Hong, X. Zhao, D.-L. Ding, M.- H. Xie, C.-D. Wu, R. Gill, K. M. Thomas and B. Chen, *Nat. Commun.*, 2011, **2**, 204; (*b*) M. C. Das, Q. Guo, Y. He, J. Kim, C.-G. Zhao, K. Hong, S. Xiang, Z. Zhang, K. M. Thomas, R. Krishna and B. Chen, *J. Am. Chem. Soc.*, 2012, **134**, 8703.
11 Y. He, R. Krishna and B. Chen, *Energy Environ. Sci.*, 2012, **5**, 9107.
12 E. D. Bloch, W. L. Queen, R. Krishna, J. M. Zadrozny, C. M. Brown and J. R. Long, *Science*, 2012, **335**, 1606.
13 S. Yang, A. J. Ramirez-Cuesta, R. Newby, V. Garcia-Sakai, P. Manuel, S. K. Callear, S. I. Campbell, C. C. Tang and M. Schröder, *Nat. Chem.*, 2014, DOI: 10.1038/nchem.2114.
14 (*a*) B. Chen, N. W. Ockwig, A. R. Millward, D. S. Contreras and O. M. Yaghi, *Angew. Chem., Int. Ed.*, 2005, **44**, 4745; (*b*) X. Lin, I. Telepeni, A. J. Blake, A. Dailly, C. M. Brown, J. M. Simmons, M. Zoppi, G. S. Walker, K. M. Thomas, T. J. Mays, P. Hubberstey, N. R. Champness and M. Schröder, *J. Am. Chem. Soc.*, 2009, **131**, 2159; (*c*) J. Cai, X. Rao, Y. He, J. Yu, C. Wu, W. Zhou, T. Yildirim, B. Chen and G. Qian, *Chem. Commun.*, 2014, **50**, 1552; (*d*) M. Li, D. Li, M. O'Keeffe and O. M. Yaghi, *Chem. Rev.*, 2014, **114**, 1343.
15 B. Chen, S. Ma, F. Zapata, F. R. Fronczek, E. B. Lobkovsky and H.-C. Zhou, *Inorg. Chem.*, 2007, **46**, 1233.
16 (*a*) R. Krishna and J. R. Long, *J. Phys. Chem. C*, 2011, **115**, 12941; (*b*) R. Krishna, *Microporous Mesoporous Mater.*, 2014, **185**, 30; (*c*) R. Krishna and R. Baur, *Sep. Purif. Technol.*, 2003, **33**, 213.

Supporting Information

A Microporous Metal–Organic Framework with Rare lvt Topology for Highly Selective C_2H_2/C_2H_4 Separation at Room Temperature

Hui-Min Wen,[a] Bin Li,*,[a] Hailong Wang,[a] Chuande Wu,[b] Khalid Alfooty,[c] Rajamani Krishna,[d] and Banglin Chen*,[a,c]

[a] *Department of Chemistry, University of Texas at San Antonio, One UTSA Circle, San Antonio, Texas 78249-0698, USA. Fax: (+1)-210-458-7428; E-mail: banglin.chen@utsa.edu*
[b]*Department of Chemistry, Zhejiang University, Hangzhou 310027, China*
[c]*Department of Chemistry, Faculty of Science, King Abdulaziz University, Jeddah, Saudi Arabia*
[d] *Van 't Hoff Institute for Molecular Sciences, University of Amsterdam, Science Park 904, 1098 XH Amsterdam, The Netherlands*

1. General Procedures and Materials. All reagents and solvents were commercially available and used without further purification. 1,2,4,5-tetraiodobenzene was prepared according to the literature procedure.[1] ^{1}H NMR spectra were recorded on a Varian Mercury 500 MHz spectrometer using tetramethylsilane (TMS) as internal standards. The coupling constants reported in Hertz. FTIR spectra were performed on a Bruker Vector 22 spectrometer at room temperature. The elemental analyses were performed with Perkin–Elmer 240 CHN analyzers from Galbraith Laboratories, Knoxville. Thermogravimetric analyses (TGA) were carried out using a Shimadzu TGA-50 analyzer under a nitrogen atmosphere with a heating rate of 5 ^{o}C min^{-1}. Powder X–ray diffraction (PXRD) patterns were measured by a Rigaku Ultima IV diffractometer operated at 40 kV and 44 mA with a scan rate of 1.0 deg min^{-1}.

2. Gas sorption Measurements. A Micromeritics ASAP 2020 surface area analyzer was used to measure gas adsorption isotherms. To remove all the guest solvents in the framework, the fresh sample of **UTSA-60** was guest–exchanged with dry acetone at least 10 times, filtered and degassed at 273 K for two days, and then at 296 K for another 2 hours until the outgas rate was 5 μmHg min^{-1} prior to measurements. The sorption measurement was maintained at 77 K with liquid nitrogen. An ice-water bath (slush) and water bath were used for adsorption isotherms at 273 and 296 K, respectively.

3. Single-crystal X-ray crystallography. The crystal data were collected on an Agilent Supernova CCD diffractometer equipped with a graphite-monochromatic enhanced Cu Kα radiation (λ = 1.54184 Å) at 100 K. The datasets were corrected by empirical absorption correction using spherical harmonics, implemented in the SCALE3 ABSPACK scaling algorithm. The structure was solved by direct methods and refined by full matrix least-squares methods with the SHELX-97 program package.[2] The solvent molecules in the compound are highly disordered. The SQUEEZE subroutine of the PLATON software suit was used to remove the scattering from the highly disordered guest molecules.[3] The resulting new files were used to further refine the structures. The H atoms on C atoms were generated geometrically.

4. Fitting of pure component isotherms

Experimental data on pure component isotherms for C_2H_2, and C_2H_4 in **UTSA-60a** were measured at temperatures of 273 K and 296 K. The pure component isotherm data for C_2H_2, and C_2H_4 were fitted with the dual-Langmuir-Freundlich isotherm model

$$q = q_{A,sat}\frac{b_A p^{\nu_A}}{1+b_A p^{\nu_A}} + q_{B,sat}\frac{b_B p^{\nu_B}}{1+b_B p^{\nu_B}} \tag{1}$$

with T-dependent parameters b_A, and b_B

$$b_A = b_{A0}\exp\left(\frac{E_A}{RT}\right); \quad b_B = b_{B0}\exp\left(\frac{E_B}{RT}\right) \tag{2}$$

The fitted parameter values are presented in Table S1. The fits are excellent for both components over the entire pressure range.

5. Isosteric heat of adsorption

The isosteric heat of C_2H_2 adsorption, Q_{st}, defined as

$$Q_{st} = RT^2\left(\frac{\partial \ln p}{\partial T}\right)_q \tag{3}$$

was determined using the Clausius-Clapeyron equation by fitting the adsorption isotherms taken at 273 and 296 K to a Langmuir expression. Figure 3c presents a comparison of the heats of adsorption of C_2H_2 in **UTSA-60a** with three other representative MOFs. The values of Q_{st} in **UTSA-60a** is lower than that for the other MOFs with coordinately unsaturated metal atoms **FeMOF-74**, **CoMOF-74**, and **MgMOF-74**.

6. IAST calculations of adsorption selectivities

The selectivity of preferential adsorption of component *1* over component *2* in a mixture containing *1* and *2*, can be formally defined as

$$S_{ads} = \frac{q_1/q_2}{p_1/p_2} \tag{4}$$

In equation (4), q_1 and q_2 are the absolute component loadings of the adsorbed phase in the mixture. These component loadings are also termed the uptake capacities. We calculate the values of q_1 and q_2 using the Ideal Adsorbed Solution Theory (IAST) of Myers and Prausnitz.[4]

Based on the IAST calculations for C_2H_2/C_2H_4 adsorption selectivities, at a total pressure of 100 kPa, the value of S_{ads} for **UTSA-60a** is in the range of 5.5 – 16, which is much higher than that for **MgMOF-74**, **FeMOF-74**, and **CoMOF-74** in the range of 1.6 to 2.2.

7. Transient breakthrough of C_2H_2/C_2H_4 mixtures in fixed bed adsorbers

The performance of industrial fixed bed adsorbers is dictated by a combination of adsorption selectivity and uptake capacity. For a proper comparison of various MOFs, we perform transient breakthrough simulations using the simulation methodology described in the literature.[5,6] For the breakthrough simulations, the following parameter values were used for **UTSA-60a**: framework density, ρ = 763 kg m^{-3}, length of packed bed, L = 0.12 m; voidage of packed bed, ε = 0.75; superficial gas velocity at inlet, u = 0.00225 m/s. The transient breakthrough simulation results are presented in terms of a *dimensionless* time, τ, defined by dividing the actual time, t, by the characteristic time, $\frac{L\varepsilon}{u}$.

The transient breakthrough simulations in Figure S9 show the concentrations of C_2H_2/C_2H_4 exiting the adsorber packed with **UTSA-60a** as a function of the dimensionless time, τ. Analogous breakthrough simulations were performed for **MgMOF-74**, **FeMOF-74**, and **CoMOF-74** using the isotherm fits parameters that are provided in our earlier work.[7] On the basis of the gas phase concentrations, we can calculate the impurity level of C_2H_2 in the gas mixture exiting the fixed bed packed with five different MOFs. Figure S10 shows the ppm C_2H_2 in the outlet gas mixture exiting an adsorber packed with **UTSA-60a**, **MgMOF-74**, **FeMOF-74**, **CoMOF-74**. At a certain time, τ_{break}, the impurity level will exceed the desired purity level of 40 ppm (indicated by the dashed line), that corresponds to the purity requirement of the feed to the polymerization reactor. The adsorption cycle needs to be terminated at that time τ_{break} and the regeneration process needs to be initiated. From a material balance on the adsorber, the amount of C_2H_4 (of the required purity < 40 ppm C_2H_2) produced during the time interval 0 - τ_{break} can be determined. Table S3 provides a summary of the breakthrough times, τ_{break} for various MOFs and the amount of C_2H_4 produced, expressed in mol per L adsorbent in fixed bed.

Notation

b_A	dual-Langmuir-Freundlich constant for species *i* at adsorption site A, $Pa^{-\nu_i}$
b_B	dual-Langmuir-Freundlich constant for species *i* at adsorption site B, $Pa^{-\nu_i}$
L	length of packed bed adsorber, m
p_i	partial pressure of species *i* in mixture, Pa
p_t	total system pressure, Pa
q_i	component molar loading of species *i*, mol kg^{-1}
q_t	total molar loading in mixture, mol kg^{-1}
q_{sat}	saturation loading, mol kg^{-1}
Q_{st}	isosteric heat of adsorption, J $kmol^{-1}$
t	time, s
T	absolute temperature, K
u	superficial gas velocity in packed bed, m s^{-1}

Greek letters

ε	voidage of packed bed, dimensionless
ν	exponent in dual-Langmuir-Freundlich isotherm, dimensionless
ρ	framework density, kg m^{-3}
τ	time, dimensionless

Subscripts

i	referring to component i
t	referring to total mixture

Scheme S1. Synthetic routes to the organic linker H_4BTAA.

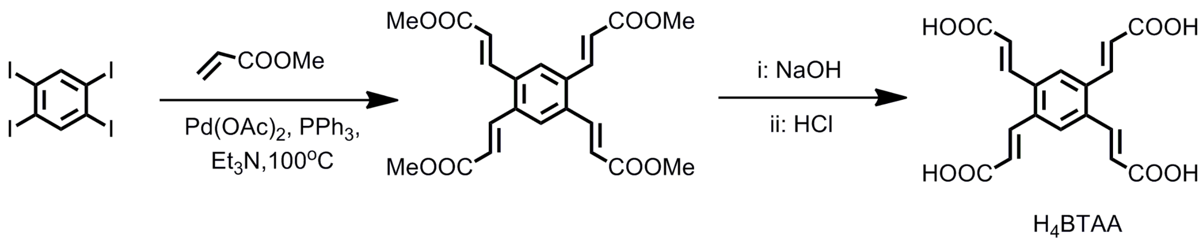

1,2,4,5-tetrakis[(methoxycarbonyl)ethenyl]benzene. In a 15 mL thick-walled Pyrex tube is placed 1,2,4,5-tetraiodobenzene (582 mg, 1 mmol), $Pd(OAc)_2$ (89.8 mg, 0.4 mmol), triphenylphosphine (210 mg, 0.8 mmol), and methyl acrylate (2 mL, 10.7 mmol), and 10 mL of triethylamine. The tube is capped and then heated at 100 ^oC for 24 h. After cooling the reactions mixtures, the precipitate was collected by filtration, washed quickly with CH_2Cl_2 for several times, and dried to afford white powder. Yield: 15% (62.1 mg). ^1H NMR (500 MHz, $CDCl_3$, ppm): δ 7.98 (d, J = 13.25 Hz, 4H), 7.73 (s, 2H), 6.41 (d, J = 13.25 Hz, 4H), 3.84 (s, 12H).

Benzene-1,2,4,5-tetraacrytic acid (H_4BTAA). 1,2,4,5-tetrakis[(methoxycarbonyl)ethenyl]benzene (496 mg, 1.2 mmol) was suspended in 30 mL THF, and then a 2M KOH aqueous solution (40 mL) was added. The mixture was stirred under reflux overnight until it became clear. After that THF was removed under reduced pressure and dilute HCl was then added to the remaining aqueous solution to acidify PH = 2. The precipitate was collected by filtration, washed with water for several times, and dried to afford white solid. Yield: 408 mg (95%). ^1H NMR (500 MHz, d6-DMSO, ppm): δ = 13.11

(s, 4H), 9.31 (s, 2H), 9.13 (s, 2H), 8.54 (s, 1H), 8.50 (s, 2H), 8.50 (s, 1H). ^{13}C NMR (d^6-DMSO, ppm): δ = 166.69, 166.65, 161.42, 156.24, 137.96, 135.20, 132.79, 132.57, 132.36, 131.95, 130.80, 130.45.

Synthesis of UTSA-60. A mixture of the organic linker H_4BTAA (5.0 mg, 0.014 mmol) and $Cu(NO_3)_2 \cdot 2.5H_2O$ (12.0 mg, 0.052 mmol) was dissolved into a 1.25 mL mixed solvent (DMF/H_2O, 1 mL/0.25 mL) in a screw-capped vial (20 mL), to which one drop of HBF_4 was added. The vial was capped and heated in an oven at 60 ^oC for 24 h. Green block crystals were obtained by filtration and washed with DMF several times to afford UTSA-60 in 65% yield. **UTSA-60** has a best formula as $[Cu_2BTAA(H_2O)_2] \cdot 2DMF \cdot 2H_2O$, which was obtained based on the basis of single-crystal X-ray structure determination, elemental analysis and TGA. Anal. Calcd for $C_{24}H_{32}N_2O_{14}Cu_2$: C, 41.20; H, 4.61; N, 4.00; found: C, 41.09; H, 4.68; N, 4.05. TGA data for loss of 2DMF and $4H_2O$: calcd: 31.16%, found: 31.25%. IR (neat, cm^{-1}): 1640, 1573, 1478, 1391, 1284, 1188, 1098, 967, 864, 701.

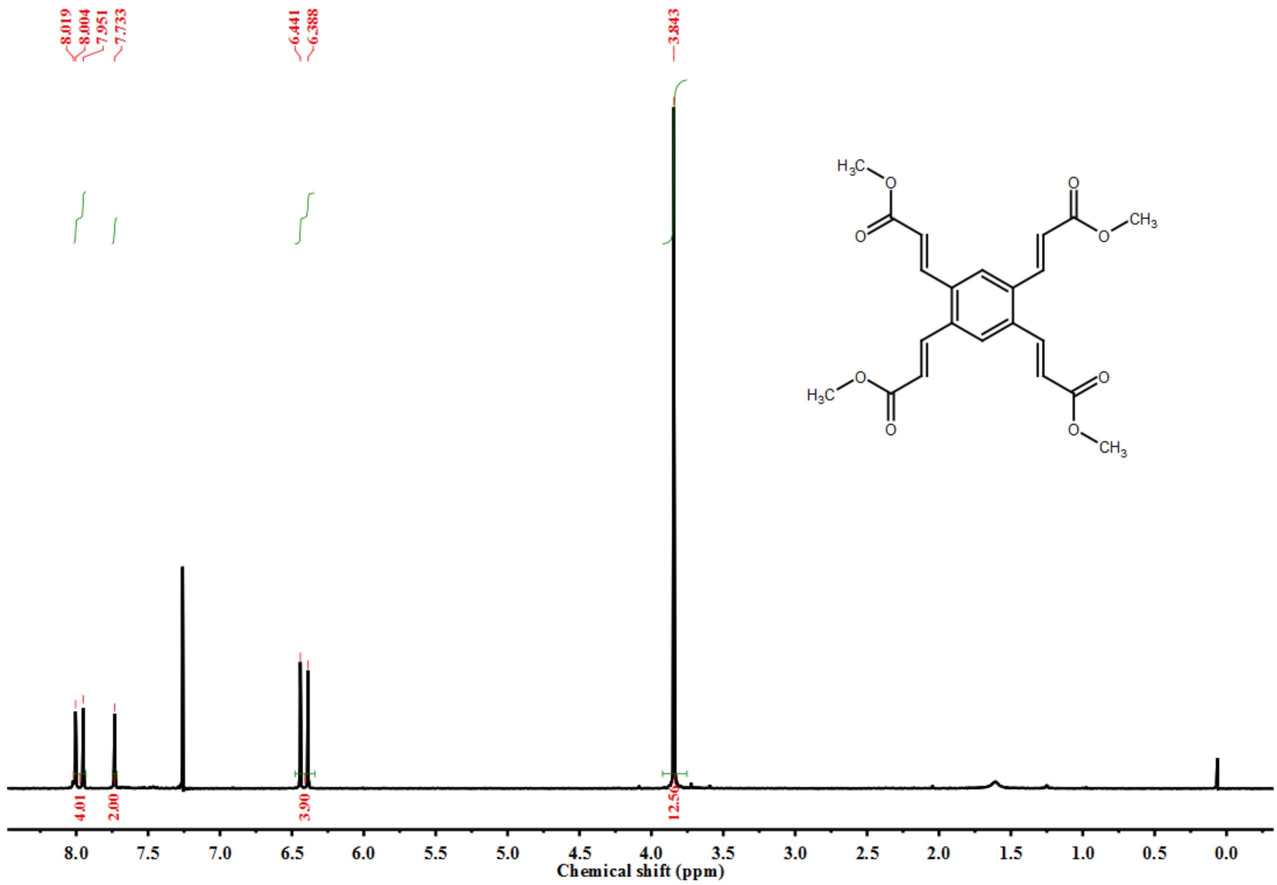

Figure S1. ^{1}H ($CDCl_3$, 500MHz) spectra of 1,2,4,5-tetrakis[(methoxycarbonyl)ethenyl] - benzene.

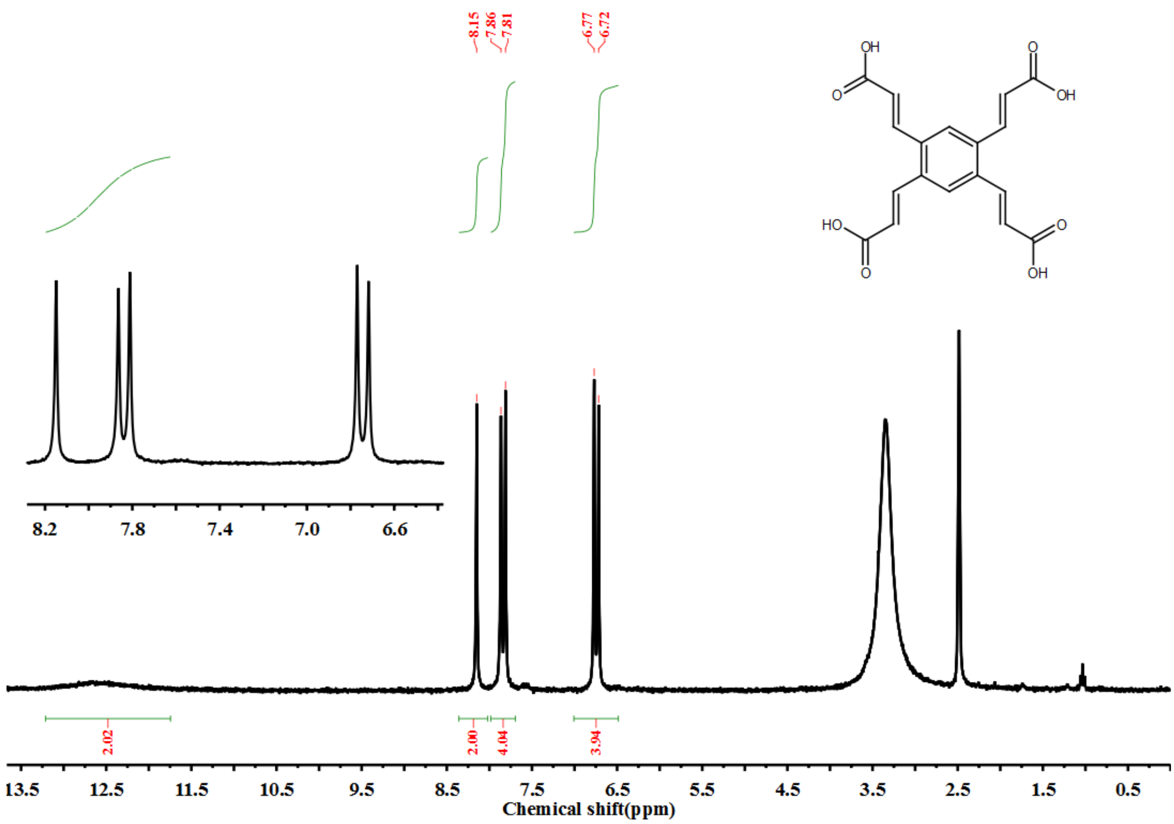

Figure S2. ^{1}H (DMSO-d_6, 500MHz) spectra of the ligand H_4BTAA.

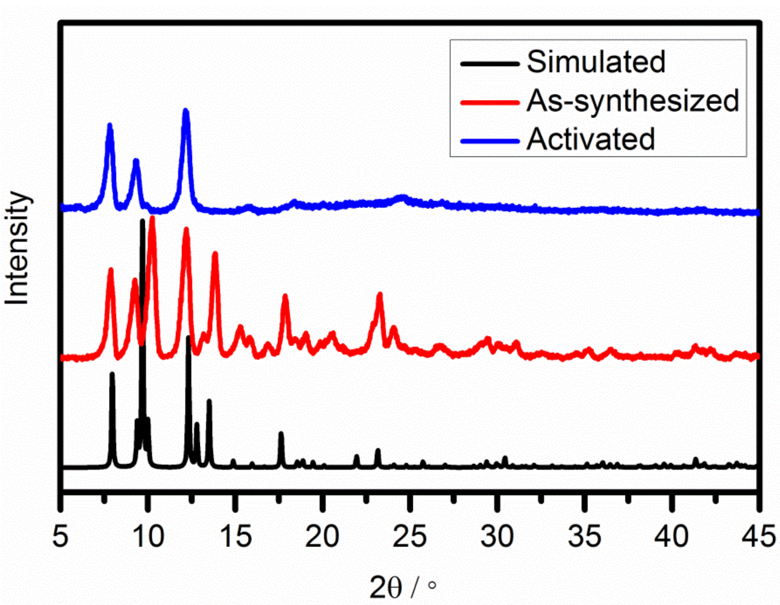

Figure S3. PXRD patterns of as-synthesized **UTSA-60** (red) and activated **UTSA-60a** (blue) along with the simulated XRD pattern from the single-crystal X-ray structure (black).

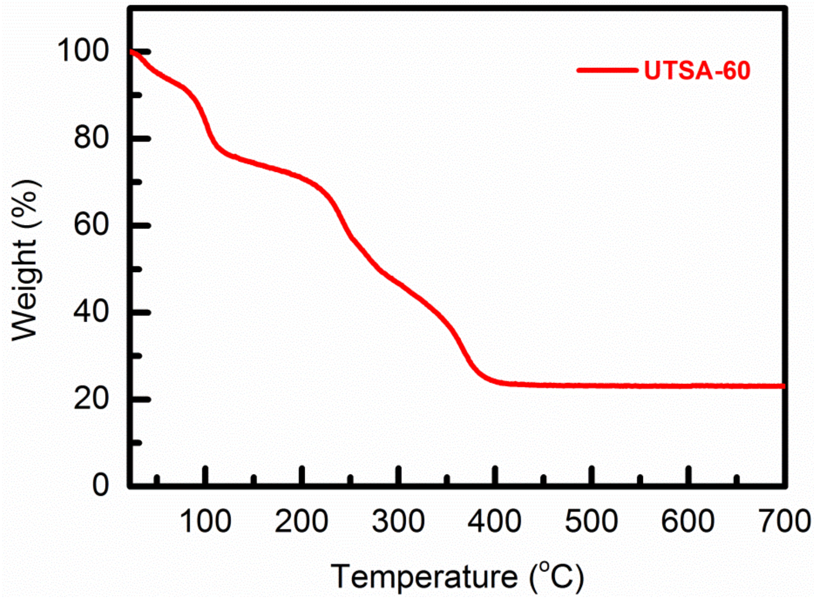

Figure S4. TGA curves of as–synthesized **UTSA-60**.

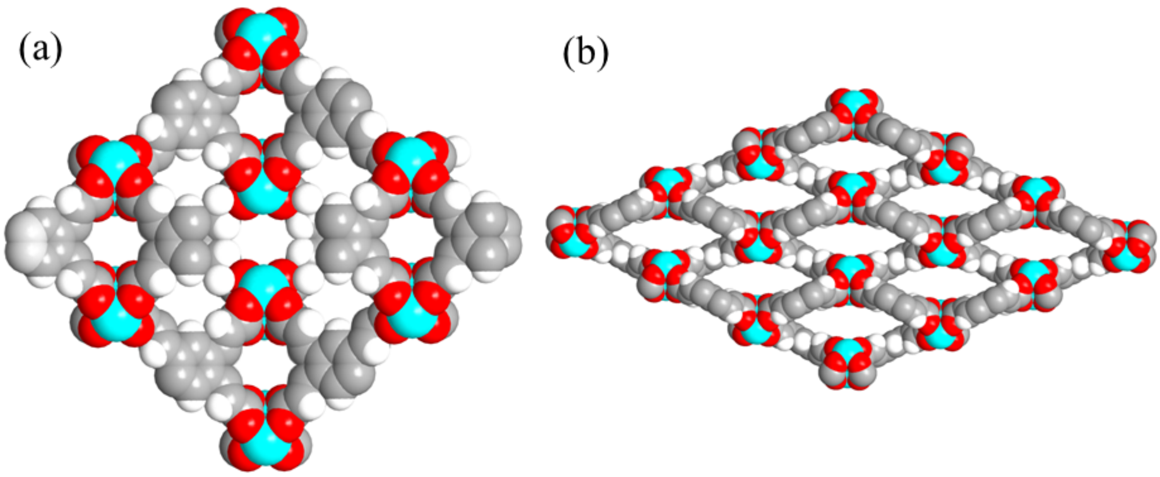

Figure S5. X-ray single crystal structure of **UTSA-60**: (a) the pore channels viewed along the *a* axes; (b) viewed along the *c* axes. Blue, red, gray, and white spheres represent Cu, O, C, and H atoms, respectively.

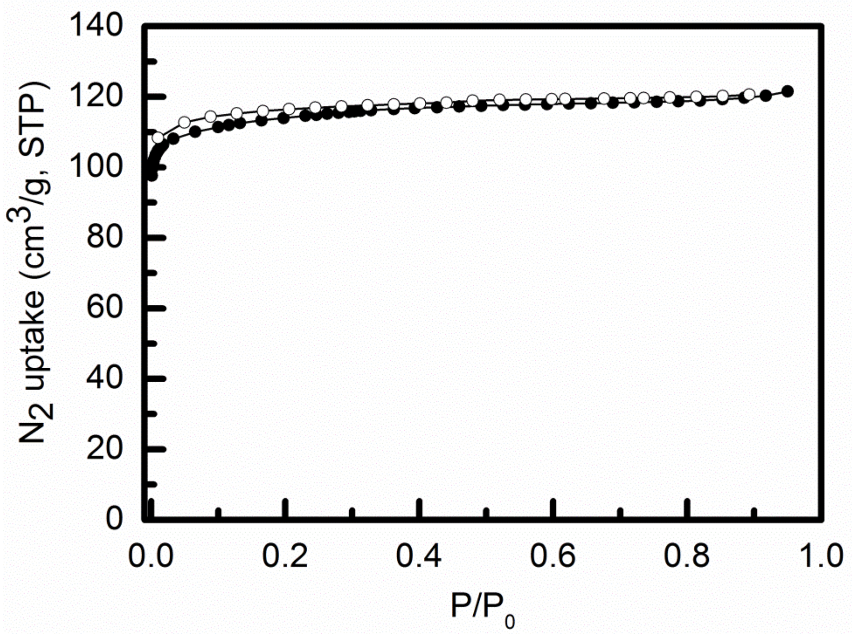

Figure S6. N_2 sorption isotherms of **UTSA-60a** at 77 K. Closed symbols, adsorption; open symbols, desorption.

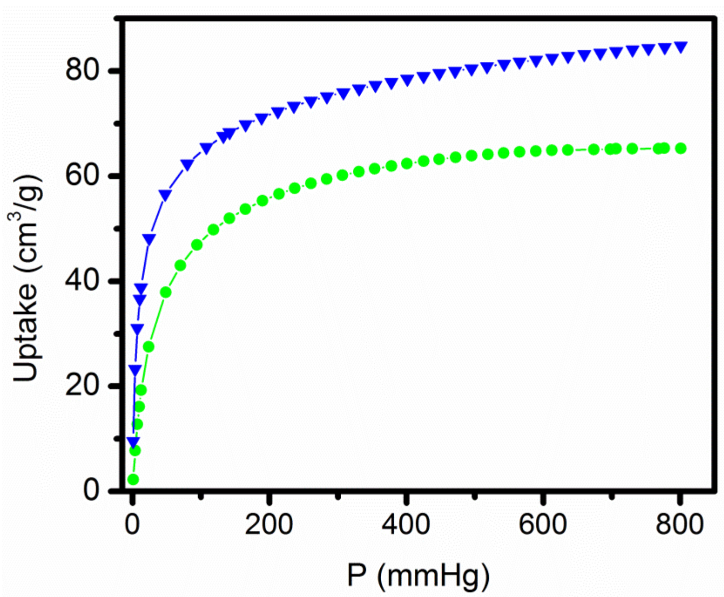

Figure S7. Single-component adsorption isotherms for C_2H_2 (blue) and C_2H_4 (green) of **UTSA-60a** at 273 K.

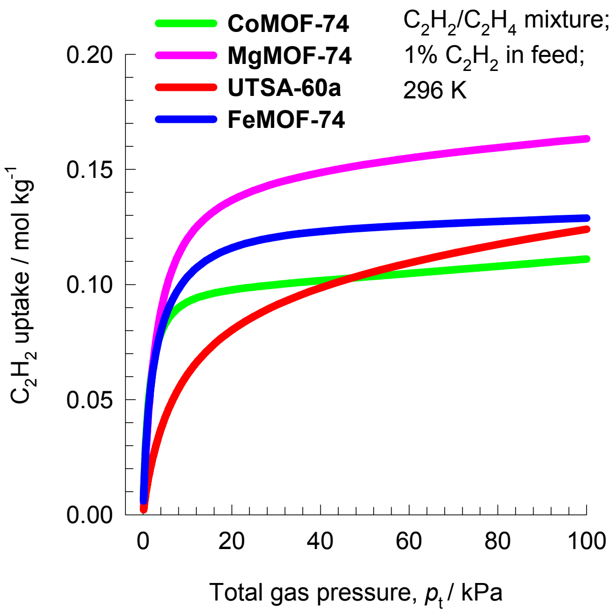

Figure S8. IAST calculations of the uptake capacity of C_2H_2 for adsorption in **UTSA-60a, MgMOF-74**, **FeMOF-74**, and **CoMOF-74** from C_2H_2/C_2H_4 mixtures containing 1% C_2H_2. The partial pressures of C_2H_2, and C_2H_4 are, respectively, p_1 = 1 kPa, p_2 = 99 kPa at T = 296 K. The data for **FeMOF-74** is at a temperature of 318 K; this is the lowest temperature used in the isotherm measurements of Bloch et al.[8]

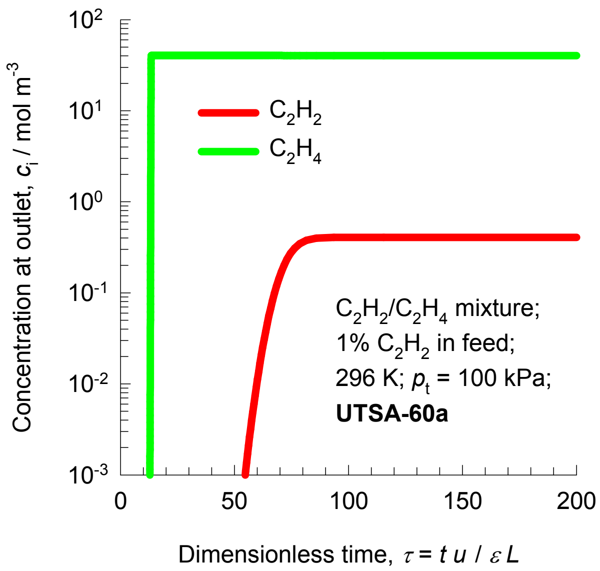

Figure S9. Transient breakthrough of C_2H_2/C_2H_4 mixture containing 1% C_2H_2 mixture in an adsorber bed packed with **UTSA-60a**. The total bulk gas phase is at 296 K and 100 kPa. The partial pressures of C_2H_2, and C_2H_4 in the inlet feed gas mixture are, respectively, p_1 = 1 kPa, p_2 = 99 kPa. For the breakthrough simulations, the following parameter values were used, as before, L = 0.12 m; ε = 0.75; u = 0.00225 m/s.

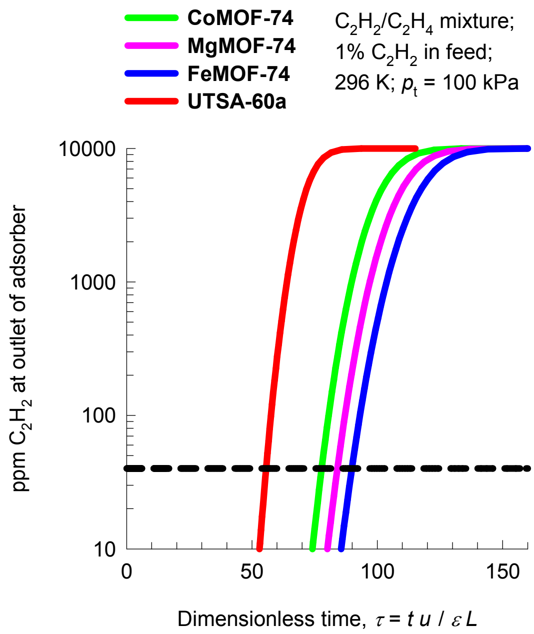

Figure S10. Ppm C_2H_2 in the outlet gas of an adsorber bed packed with **MgMOF-74**, **CoMOF-74**, **FeMOF-74**, and **UTSA-60a**. The total bulk gas phase is 100 kPa; the partial pressures of C_2H_2, and C_2H_4 in the inlet feed gas mixture are, respectively, p_1 = 1 kPa, p_2 = 99 kPa. The temperature is 296 K for all MOFs except **FeMOF-74** for which the chosen temperature is 318 K.

Table S1. Crystallographic data and structure refinement results for **UTSA-60** (from single-crystal X-ray diffraction analysis on the as-synthesized sample).

	UTSA-60
Formula	$C_{18}H_{14}Cu_2O_{10}$
Formula weight	517.37
Temperature/K	100.00(19)
Crystal system	orthorhombic
Space group	Imma
a (Å)	18.6261(10)
b (Å)	22.1934(9)
c (Å)	10.0062(8)
α (°)	90.00
β (°)	90.00
γ (°)	90.00
V (Å^3)	4180.7(4)
Z	4
D_{calcd} (g cm^{-3})	0.822
μ (mm^{-1})	1.493
F(000)	1040.0
Crystal size/mm^3	0.40 × 0.32 × 0.20
GOF	0.948
R_{int}	0.0338
R_1, wR_2 [I>=2σ (I)]	0.0639, 0.1574
R_1, wR_2 [all data]	0.0806, 0.1700
Largest diff. peak and hole (e Å^{-3})	0.568, -1.958

Table S2. Dual-Langmuir-Freundlich parameter fits for **UTSA-60a**.

	Site A				Site B			
	$q_{A,sat}$ mol kg^{-1}	b_{A0} $Pa^{-\nu_i}$	E_A kJ mol^{-1}	ν_A dimensionless	$q_{B,sat}$ mol kg^{-1}	b_{B0} $Pa^{-\nu_i}$	E_B kJ mol^{-1}	ν_B dimensionless
C_2H_2	3.3	2.35×10^{-9}	31	0.86	3.1	2.12×10^{-19}	68	1
C_2H_4	2.3	2.82×10^{-13}	46	1.1	0.75	3.17×10^{-36}	146	1.7

Table 3. Breakthrough calculations for separation of C_2H_2/C_2H_4 mixture containing 1 mol% C_2H_2 at 296 K. The data for FeMOF-74 is at a temperature of 318 K; this is the lowest temperature used in the isotherm measurements of Bloch et al.[8] The product gas stream contains less than 40 ppm C_2H_2.

	Dimensionless breakthrough time τ_{break}	C_2H_4 produced during 0 - τ_{break} mol L^{-1}
CoMOF-74	77.4	1.97
MgMOF-74	84	3.93
FeMOF-74	89.6	3.57
UTSA-60a	55	5.1

References

1. L. M. Daniell. *J. Org. Chem.*, 1984, **49**, 3051–3053.

2. Sheldrick, G. M. Program for Structure Refinement. Germany, **1997**.

3. Spek, L. PLATON: The University of Utrecht: Utrecht, The Netherlands, **1999**.

4. A. L. Myers and J. M. Prausnitz, *A.I.Ch.E.J.*, 1965, **11**, 121–127.

5. R. Krishna and J. R. Long, *J. Phys. Chem. C*, 2011, **115**, 12941–12950.

6. R. Krishna, *Microporous Mesoporous Mater.*, 2014, **185**, 30–50.

7. Y. He, R. Krishna and B. Chen, *Energy Environ. Sci.*, 2012, **5**, 9107–9120.

8. E. D. Bloch, W. L. Queen, R. Krishna, J. M. Zadrozny, C. M. Brown and J. R. Long, *Science*, 2012, **335**, 1606–1610.